Fracture strength of glass chips for high-pressure microfluidics

Martin Andersson[1], Klas Hjort and Lena Klintberg

Department of Engineering Sciences, Uppsala University, Box 534, 751 21 Uppsala, Sweden
[1]Corresponding author: martin.andersson@angstrom.uu.se

Abstract

High-pressure microfluidics exposes new areas in chemistry. In this paper, the reliability of transparent borosilicate glass chips is investigated. Two designs of circular cavities are used for fracture strength tests, either 1.6 mm wide with rounded corners to the fluid inlets, or 2.0 mm wide with sharp inlet corners. Two kinds of tests are done, either short-term, e.g. pressurization to fracture at room temperature, or as long-term, fracture at constant pressurization for up to 1 week, in the temperature region 11 to 125 °C. The speed of crack fronts is measured using a high-speed camera. Results show fracture stresses in the range of 129 and 254 MPa for short-term measurements. Long-term measurements conclude the presences of a temperature and stress dependent delayed fracture. For a reliability of 1 week at 11 to 38 °C, a pressure limit is found at the lower end of the short-term measurements, or 15% lower than the average. At 80 °C, this pressure limit is 45% lower. Crack speeds are measured to be 10^{-5} m/s during short-term fracture. These measurements are comparable with estimations based on slow

crack growth and show that the growth affects the reliability of glass chips. This effect is strongly affected by high temperatures, thus lowers the operating window of high-pressure glass microfluidic devices.

1. Introduction

High-pressure microfluidics broaden the use of high-pressure chemistry to new applications. Greatly favored by scaling laws, microfluidic chips can contain fluids at high pressure, thereby enabling new methods and applications for high pressure fluids [1]. Aqueous fluids have commonly been part of high-pressure fluid systems, for example in the use of extracting lignin oxidation products from H_2O streams into CO_2 [2], or to study micro emulsions [3]. Supercritical water, as well as hot water, has also been explored [4]. Transparent systems, such as of glass, offer optical access, and a number of applications rely on them [5-7].

Yet, the combination of large stresses and water containing fluids is infamous for causing environmentally driven crack growth in glass, leading to delayed fractures [8-10]. In this paper, the effect of such crack growth in high-pressure microfluidic glass chips is investigated.

High-pressure chemistry requires a large operation window in terms of pressure and temperature. This puts high demands for the materials used, and as the field of interest often is found at the borders of what is currently possible, it is necessary to stretch the limit of the strengths in microsystems. Anodic bonded glass and silicon based devices have been made that can operate at 250 bar, or 25 MPa, at 400 °C with supercritical water, and 450 bar at room temperature [4]. A few mechanical evaluations have been made on fusion bonded borosilicate glass devices by short-term pressurization of plugged channel inlet structures to fracture [11-12]. Using H_2O at rate of 2000 µL/min, 120 µm wide tubular channels resulted in fracture pressures up to 690 bar [11]. Semicircle-shaped, 580 µm wide and 380 µm deep, channels resulted in lower pressures, in the range of 120 to 260 bar. Tests done with CO_2 resulted in slightly higher pressures, indicating an environmental dependence on fracture strength. In one other study, 600 µm wide semicircle-shaped channels resulted in pressures in the range of 120-320 bar at pressurization rates of 0.3 bar/s [12].

Slow crack growth in brittle materials, such as glass, can occur even at moderate stress levels if strained crack tips are exposed to reactive species [9]. Commonly, this subcritical growth has been investigated at rates in the range of 10^{-10} to 10^{-4} m/s [8]. This environmentally driven effect has rarely been described as a concern in the

field of microfluidics, since chips seldom are under high stresses while being in contact with chemical species. However, its contribution to failure in microsystem silicon devices has been noted in reliability studies [13]. Crack growth in silicon devices has been measured down to 10^{-13} m/s [14].

For most applications, a long-term durability at high pressures is required. As only short-term measurements have been done on fusion-bonded borosilicate glass, and environmentally driven crack growth typically can cause delayed fracture under these conditions, this stresses the need to investigate the effect of long-term pressurization.

In this work, the reliability of fusion-bonded glass devices is investigated by both short-term and long-term pressurization at different temperatures and pressures. For systems to be useable for a larger set of applications, it must be defined under which conditions these systems can operate under an extensive period of time, and when slow crack growth starts to become a problem.

2. Background

The fracture toughness can be estimated using the double cantilever beam model [15]. Two bended beams are clamped rigid at one point that defines a crack tip, and are held clamped beyond this point. Using the Griffith energy criterion to calculate an energy release rate G_I, the fracture toughness can be derived. To be applicable, the crack tip must be sharp and the point beyond the crack tip must be considered long. For a circular pressurized cavity, with both top and bottom bulging, an expression for the energy release rate, G_I, can be made, given that the crack front is uniform around the cavity [15-16],

$$G_I = \frac{6P^2r^4(1-\nu^2)}{32Eh^3}\left(1+\frac{8\alpha_s h^2}{3r^2(1-\nu)}\right) \quad (1)$$

P is pressure, r is the radii from the center of the cavity to the crack tip, h is the plate thicknesses, E is the Young's modulus, and ν the Possion's ratio. α_S is a sheer coefficient normally set to 1.5 [15]. For borosilicate glass, E typically is 64 GPa and ν is 0.2 [17]. For the glass chips used in this study, figure 1, the structures have inlets leading to a central cavity. (1) relies on a circular geometry and is therefore only approximate descriptive of the situation in this study. Fracture toughness is often discussed in terms of a stress intensity factor, K_I, and for linear elastic materials, G_I can be converted to K_I, by [15],

$$K_I = \sqrt{\frac{EG_I}{1-\nu^2}} \quad (2)$$

The stress intensity factor is large at high stress locations and where cracks are present. For a circular cavity, the highest

stresses are found at the cavity edges. Structures formed by single-sided isotropic etching, figure 1(c), will have stress concentrations at the structure border where the wafers meet [12]. From this cross sectional point, a cavity edge curve, C, can be formed along the structure. The bond interface, found between direct bonded wafers, is associated with flaws, and a distribution of flaws with different crack lengths will be present along C. As the locally highest combination of flaw size and stress results in fracture onset, the strength of the device will follow the Weibull distribution and can be described in the following form,

$$p_f = 1 - \exp\left[-\int_C \left(\frac{\sigma_C(s)}{\sigma_0}\right)^m ds\right] \qquad (3)$$

where the probability of fracture, p_f, is expressed as a function of the stress along C with $\sigma_c(s)$ as the stress on C at position s [18-19]. σ_0 and m are characteristic stress and Weibull modulus, respectively.

By experiments, it is found that there is an exponential dependence between crack velocity and stress intensity factor in glass [9]. Because of this, a very small crack can under constant load lead to a delayed fracture given the right timescale. By using chemical reaction rate theory, environmental crack growth can be described [20]. As stress is applied to the crack tip, the strain stretches the silicate bonds of the glass and lowers the activation energy of reaction with a surrounding chemical species. As the species, most often described for water, reacts with the bond, a propagation of the crack occurs. The crack speed can then be related to K_I by the reaction rate V according to

$$V = V_0 a_{H_2O} \exp\left[\frac{-H + bK_I}{RT}\right] \qquad (4)$$

a_{H_2O} is the activity of water, V_0 is a constant, H is the activation energy of the reaction, b relates to the activation volume of the chemical species, R is the gas constant and T is the temperature. For a borosilicate glass, H is 129 kJ mol^{-1}, $\ln V_0$ is 3.5 and b is 0.200 $m^{5/2}$ mol^{-1} [20]. It is well worth noticing that (4) does depend on activity. Therefore, crack growth can occur even if moisture levels are low. Subcritical crack growth can occur in vacuum, but by a different mechanism and at higher K_I [22]. For a cavity under constant pressure, the time of fracture will ultimately be determined by the time, t, it takes for the crack front to progress,

$$t = \int_{r_c}^{\infty} \frac{1}{V}\, dr \qquad (5)$$

where r_c is the radius of the cavity. By the combined expression of (1), (2) and (5), an estimate of the time of fracture can be made.

Growth rate studies of slow cracks for water at different stress intensity factors, K_I, and temperatures, have been made for several different glass compositions. At a K_I around 0.4 MPa $m^{1/2}$, both soda-lime and borosilicate glass at 25 °C show a crack growth rate in the order of 10^{-7} m/s, but for silica at room temperature, the velocity is less than 10^{-10} m/s [21]. If the temperature is increased to 90°C, velocities in the order of 10^{-5} m/s are seen at the same K_I for soda-lime glass.

3. Materials and method

3.1 Design

The chips have a circular cavity placed in the center of the chip, figure 1. Two inlets on the edges connect the cavity. Two different designs were studied. On the first, design 1, the cavity and channel depth is 100 µm. The cavity is 2 mm in diameter and the inlet width is 190 µm. In this design, the edge is sharp where the inlet meets the cavity. On the second, design 2, the first 2.5 mm of the inlets have a depth of 170 µm. The rest of the inlet channels and the cavity have been etched to a depth of 50 µm. The cavity diameter is 1.6 mm and there is a fillet with a radius of 250 µm where the inlet meets the cavity, giving it a rounded edge. The width of the channels at the cavity is 130 µm. All chips have a total thickness of 2.2 mm.

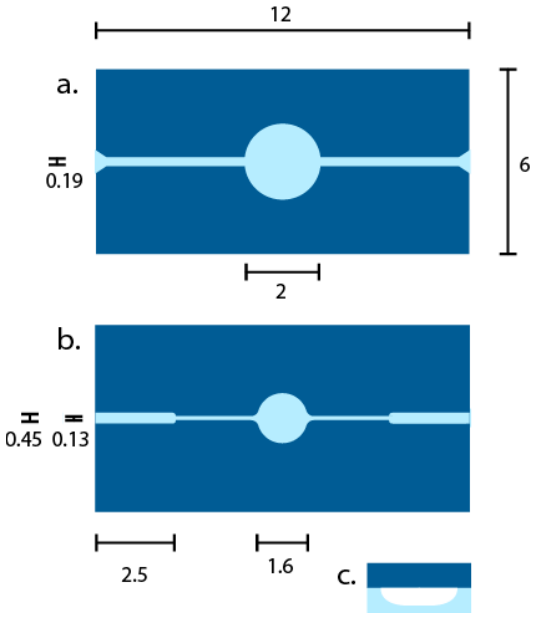

Figure 1. Design 1, (a), and design 2, (b), scale in mm. The cross section geometry of the channels, (c), is not to scale.

3. 2 Measurements

Measurements have been carried out by two different test schemes to determine the presence of delayed fracture in the glass chips. The first method consists of a fast, here defined as a short-term, measurement of the fracture strength. It is done by rapidly increasing the pressure to the point of fracture. By this method, a reference value of the strength can be found, both for water and for CO_2 as the pressurizing medium. The second method employed, here defined as long-term measurements, is done to see if delayed fracture occurs and is preformed by having a constant pressure applied to the chip until it fractures, alternatively, survives for one week. As environmental crack

growth is dependent on both stress and temperature, measurements are done under different temperatures and pressures. H_2O was used as a pressurizing medium. The activity, a_{H2O}, can then be taken as unity, which maximizes the effect and simplifies conclusions.

By preforming short-term measurements on the two different designs, differences in geometry can be resolved. Design 1 has sharp corners to the cavity inlets where as design 2 has a fillet, which will result in different $\sigma_c(s)$ along the edge curve C. A high-speed camera is used to study the crack front of short-term measurements as a fracture develops. By such method, the fracture mechanism can be studied.

The test system consisted of two high-pressure syringe pumps (100DM, ISCO Teledyne), a cooling bath with heat stage, and a high-speed camera mounted on a stereoscope. Deionized and sonicated H_2O was held at 20 °C is in one pump and CO_2 (99.9995%, AGA) was held at 4.5 °C and 60 bar in the other. Pressurized CO_2 was flowed trough a column containing dried silica gel loaded with a moisture sensitive dye to determine the presence of moisture in the test system. Color and weight changes were checked.

The chips were mounted on two different temperature controlled stages, either a 11 °C aluminum plate partially submerged in a 20 L bath cooled by a compressor (RK-20, Lauda), or a heat stage consisting of Kantal wirings on AlN plates. 4-point temperature measurements where done right next to the chips with a Pt-100 sensor connected to a data acquisition device, DAQ, (34970A, Aligent). Thermal grease was applied between chips, temperature sensor and heat stages. A glass cover was applied over the chips to hinder external convection. Silica capillaries were utilized as interface between the chips and a stainless steel tube (inner diameter 254 µm) connected via needle and check valves to the pumps. The high-speed camera (Miro 320, Phantom Vision) was mounted on a 2x magnification stereoscope (SMZ800, Nikon). A micro controller (Uno, Arduino) was used to trigger the high-speed camera by sending a trigger signal when a pressure drop was detected on the analog pressure transducer port of the high-pressure pump. To monitor and log data, the high-pressure pumps, DAQ, and micro controller was connected to a computer with a software interface (Matlab, Mathworks).

Chips from both design 1 and design 2 were tested by the short-term method. The chips where first pressurized to 80 bar and then ramped to failure at an approximate speed of 0.5 bar/s. Chips that failed before 80 bar had in all cases confirmed leakage between the glue and the capillary inlet, and were

discarded from the study. The high-speed camera was set to 5,000 frames/s. Using the camera software, the velocity of the crack front in the video could be calculated. The image data, 768x576 pixels, was processed in an image analysis software (Fiji Life-Line version 20151222, Fiji) using first a background subtraction (rolling ball radius of 25 pixels) and then a contrast and brightness adjustment.

Long-term measurements of chips from design 2 at different pressures were done using H_2O. Pressurization was first done to 130 bar at a rate of 0.5 bar/s while being held at 20 °C. Chips that did not fracture at this pressure within 2 min were depressurized and selected for long-term based measurements. Long-term measurements were taken at 4 different temperature levels; 11, 38, 80 and 125 °C. The pressures were selected to resolve data points within the timeframe of the study, between 5 min and 168 h, corresponding to a life-time of one week. Some of the samples that did not fail after 168 h were depressurized and the fracture strength was measured using the short-term pressurization with H_2O as the pressure medium.

The fracture surfaces were studied with a scanning electron microscope (1550, Zeiss) and height data was recorded using white light interferometry (Wyko NT1100, Veeco). The stresses in the chip were simulated using finite element analysis (Comsol Multiphysics 5.2, Comsol) of 3D models using a maximum element size of 20 μm. Weibull analyses were preformed using the maximum likelihood estimation by the wblfit function in in Matlab. Using a 99% level of confidence, σ_0 and m could be extracted as intervals for each measurement series.

3.3 Fabrication

The glass chips were manufactured in a clean room using lithography, wet etching and thermal bonding. First, 1.1 mm thick, 4 inch, borosilicate (Borofloat 33, Schott) wafers were cleaned in a megasonic cleaning bath (PCT Systems Inc.) for 1.5 min with a solution of 25 wt. % KOH at 65 °C. After rinse in deionized water, the wafers were immersed in 69 wt. % HNO_3 at 80 °C for 10 min, and then rinsed again, followed by spin-drying in combination with nitrogen blowing to get rid of all moisture. Molybdenum was sputtered (CS730S, Von Ardenne) at 1,000 W for 240 s on both sides of the cavity wafer, which gave a 1 μm thick etch mask. To structure the wafer, a spray resist mask was added onto the molybdenum. This began with adding an adhesion promoting primer, HMDS, which was applied using a primer furnace (Star 2000, Star). The spray resist (AZ9260, Micro Chemicals) was 12 μm thick and was applied on both sides using a spin-spray

coater (101, EVG). Soft baking was first done at 95 °C on a hotplate for 2.5 min for the first deposition and then in an oven for 20 min for the backside deposition. Using UV-lithography, structuring was completed using a developer (AZK400, Microchemicals) with a mixing ratio of 1:4 of developer and water. After completion of the resist mask, the molybdenum mask was structured by etching in a solution of 11.5 wt. % HNO_3 and 19 wt. % HCl for 3 min. The resist was then left on and hard baked for 20 min at 120 °C before the wafers were etched in 49 wt. % HF at room temperature to the desired depth. The resist was stripped by acetone and isopropanol. This was followed by a 1,000 W O_2 plasma (Plasma Processor 300, Tepla) for 10 min and removal of the molybdenum mask in the 11.5 wt. % HNO_3 and 19 wt. % HCl solution.

Cleaning and activation before bonding is preformed by first exposing both the structured wafers and the unstructured lids for 10 min in an O_2 plasma at 1,000 W. This is followed by 1.5 min in 25 wt. % KOH at 65 °C in a megasonic cleaning bath. The wafers are then immersed in 69 wt. % HNO_3 at 80 °C for 15 min and then rinsed in H_2O for 5 min. After spin-drying with nitrogen, the wafers are bonded. The wafers are treated in a vertical oven (Micro TF-6, Koyo Lindberg) at 625 °C with a dwell of 6 h and a ramp up/down of 1 °C/min. As a last step, the bonded wafers were diced (DAD 361, Disco). Design 1, having all structures at the same depth, was made using one mask and one structuring. As design 2 have two different etch depths, it was done in two steps by first creating the first mask, then do structuring of the cavity and small inlets. This is followed by stripping the entire used mask and then applying a new mask for the structuring of the outer inlets.

3.4 Chip assembly

Visual inspection of the chips was done and those that showed defects, such as particles or black spots in the bond interface, were sorted out of the study. The yield was higher than 95%. In this study, 1 wafer of design 1 and 3 wafers of design 3 were used. Within the designs, chips were randomized. Silica capillaries where inserted into the side of the chips. For design 2, polyimide coated silica capillaries having an outer diameter of 150 µm and an inner diameter of 75 µm were used. For design 1, polyimide coated capillaries of 105 µm outer diameter and 40 µm inner diameter were used, but here the polyimide was burned off at the capillary tip to allow insertion into the 90 µm deep inlet. The capillaries were then glued to the chips using a 2-component epoxy glue (Araldite Rapid, Huntman Advanced Materials), which also was used to mount the chips on

100 µm thick glass cover slides. The glue was allowed to cure for at least 48 h under dry environment. In both designs, only one inlet was used, and the other was plugged by glue.

4. Results

4.1 Fracture measurements

The measured probability of fracture as a function of pressure for short-term measurements is shown as a Weibull plot in figure 2.

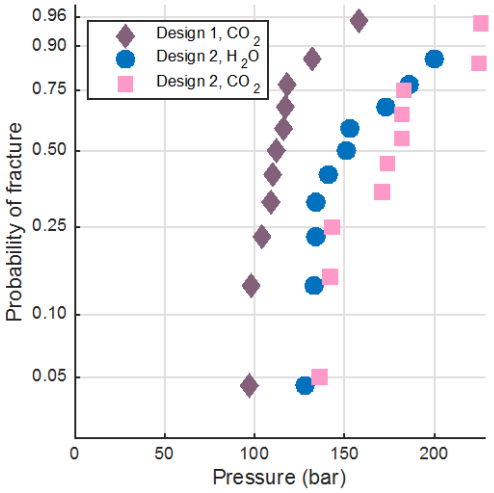

Figure 2. The probability of fracture as a function of pressure for design 1 and design 2 using CO_2 and H_2O as pressurizing media for the short-term measurements.

Pressurizing using CO_2 resulted in that fractures occur at pressures between 98 and 158 bar for design 1 and between 136 and 226 bar for design 2. The medians for the two designs are 112 and 178 bar, respectively. At seconds before of fracture, a crack front develops, figure 3. It expands from the cavity edge and the circular shape is distorted at the inlets. Measured on 4 samples, the crack front speed is 36 ± 10 µm/s, e.g. 10^{-5} m/s. Moisture tests on the system pressurized with CO_2 indicated the presence of H_2O in the system and pressurizing fluid as a color change of the silica occurred as well as a weight increase.

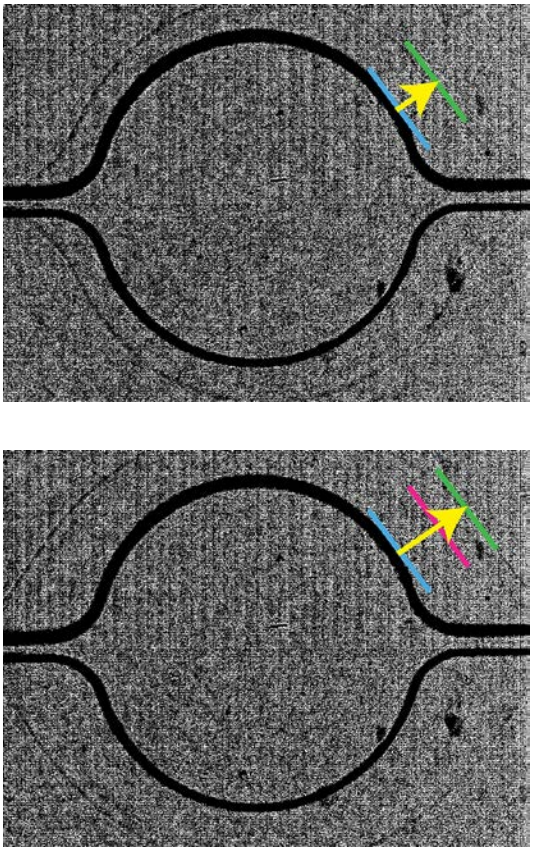

Figure 3. **A cavity from a design 2 chip, being pressurized using CO_2. A crack front (green) is seen expanding around the cavity 3.45 s before the fracture (top). The crack front develops from the cavity edge (blue) it the outwards direction (yellow arrow). In the frame before fracture (bottom), the position of the crack front at the previous image is marked (purple). The fracture pressure was 143**

bar and image processing has been applied to enhance the crack front more clearly.

The short-term measurements of design 2, using H_2O as the pressurizing fluid, resulted in fracture pressures between 128 and 238 bar with an median of 151 bar. The median difference is hence 27 bars lower for H_2O compared to CO_2. Long-term measurements for design 2 are shown in figure 4. Within the 168 h time scope of study, a threshold pressure can be determined, and above this critical value, delayed fracture is seen. This threshold pressure, as a function of temperature, is shown in figure 5. At 38 °C, the critical pressure is 129 bar and at 80 °C it is 85 bar. Compared with the median of short-term measurements, this translates to 15% and 45% lower strength, respectively. Three samples from design 2 that did not fracture after being held at high pressure for 168 h were retested according to the method used for short-term measurements and showed then an average strength of 210 bar.

The long-term measurements of the time of fracture are compared with estimates, as calculated by (5), in a correlation plot, figure 6. In general, the measured time of fracture either occurs around or before the estimated time of fracture.

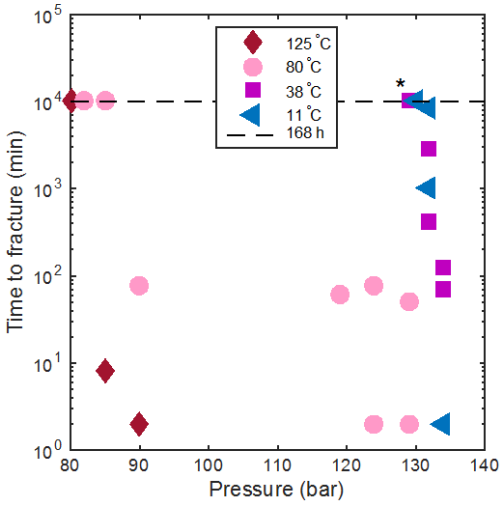

Figure 4. The time to fracture for different pressures at 11, 38, 80, 125 °C is shown for design 2. The (*) indicate a double point on the dashed line at 129 bar and 38 °C. The dashed line indicates the end of the study period.

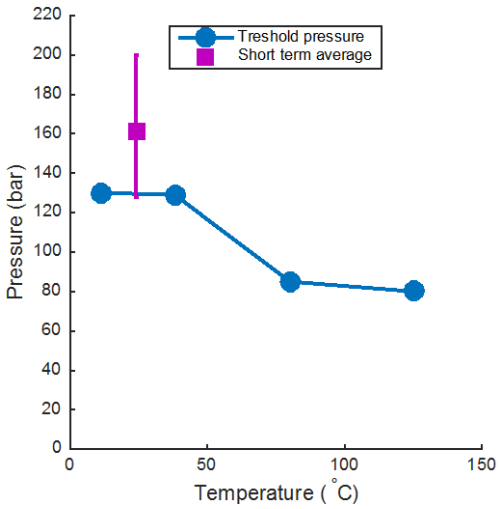

Figure 5. The temperature dependence of the 168 h threshold pressure. The average short term fracture pressure of design 2 together with error bars indicating the highest and lowest values is included as a reference.

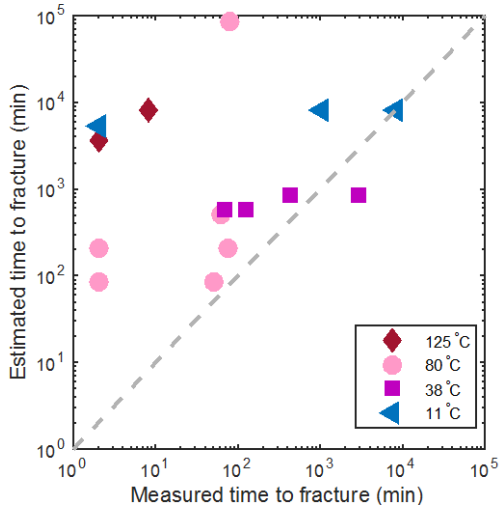

Figure 6. The time of fracture for the long-term measurements is shown as a correlation plot between measured values and estimated, calculated, values. Values either fall close to the dashed correlation line or to the left.

4.2 Modeling and stress estimation

Modeling of the stress for both designs showed that large differences in stress are present. The cavity and inlets of design 1 is shown as a top view in figure 7(a). It shows stress concentration points located where the inlets meet with the cavity, along the cavity edge curve C. The stresses at these 4 points are about twice as high as on the circular arcs of the cavity, being 111 MPa at the arcs and 213 MPa on the stress concentration points for a cavity pressurized to 133 bar. The curved design in design 2 avoids the stress concentrations and here, the stress is uniform on the cavity arc, as seen in figure 7(b). By the use of the developed FEM model, the maximum stress, along C at a given fracture pressure, have been calculated for the two designs. Using the fracture pressures presented in figure 2, the corresponding stresses of these measurements are presented, as a Weibull plot, in figure 8. Given a 99% level of confidence, the characteristic fracture stress, $\sigma_{0,}$ of the estimated Weibull distribution for design 1 and 2, tested under CO_2, is found in the intervals 174 to 225 MPa and 167 to 219 MPa, respectively. The Weibull modulus, m, is 6,4 and 6,3, respectively. These intervals do overlap and no clear distinction can be made between them. While instead testing with H_2O instead of CO_2 for design 2, $\sigma_{0,}$ is found between 149 to 210 MPa. As this interval overlaps with those of H_2O, no significant difference in fracture strength between CO_2 or H_2O was found.

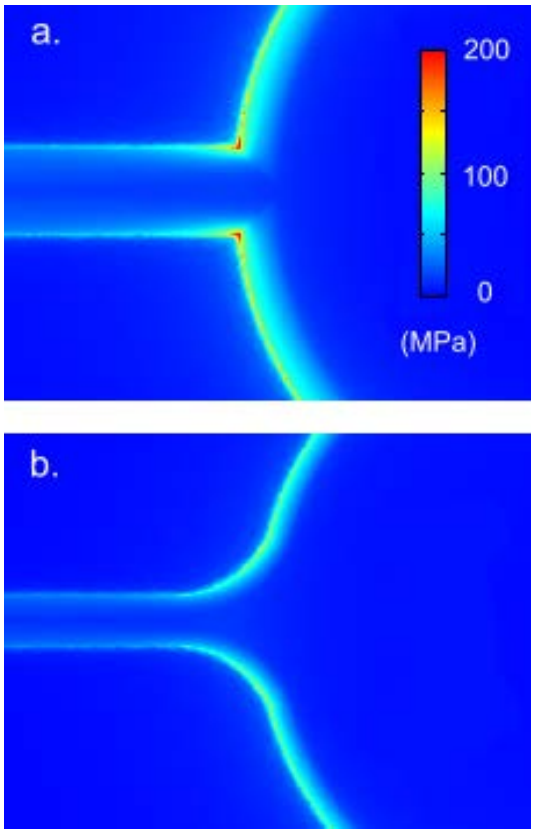

Figure 7. Surface plot of stress concentrations at the cavity and inlet for design 1 (a) and design 2 (b) calculated at 133 bar. For design 1 and 2, the maximum stress is 213 MPa and 133 MPa, respectively.

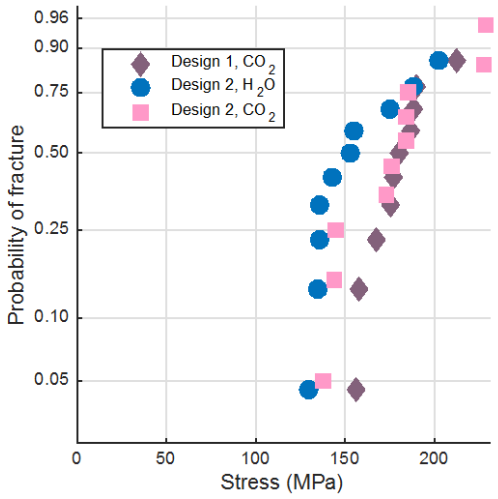

Figure 8. Probability of fracture as a function of the maximum calculated stress for the two designs using H_2O for design 1 and CO_2 as well as H_2O for design 2.

4.3 Fracture characterization

At fracture, the chips split apart forming two fracture surfaces, figure 9. The flat region in the center of the cavity, figure 9(b) is the unbonded lid of the cavity and this corresponds to the bond interface plane. The fracture surface around the cavity originates from this plane and then slopes downwards 20 µm to a fracture plane, which conclude that delamination is not occurring but rather that the crack develops in the bulk material. Where the inlets meet the cavity, the downward slope is not notable and no clear transition between the bonded fracture surface and the unbonded regions of the cavity and inlet is seen. Around this area, the topography difference between fracture

surface and lid is 4 µm. The fracture surfaces are smooth and do not show any clear variations in the surface topography over approximately the first 1 mm away from the cavity. As no change is seen, no signs of different crack growth mechanisms are observed. The fracture surface further away than 1 mm, close to the edges of the chips, show ripple marks and deviates upwards.

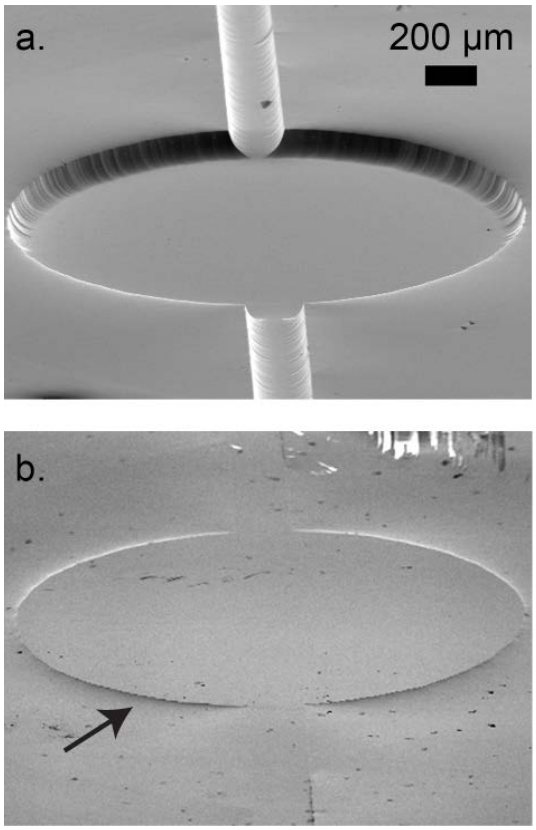

Figure 9. The fracture surfaces from a chip after failure, design 1. The etched cavity can be seen on one of the sides (a), and the cavity lid (b) on the other. Indicated by an arrow, a slope away from the lid can be seen.

5. Discussion

By comparing the results shown in figure 5, a reduction of more than half the strength can be seen when the chips are held under constant pressurization for a week at a temperature above 80 °C. The survivability of glass chips is not only a function of pressure, but also on time and temperature. This is fully consistent with what is known about environmental crack growth [9].

The short-term calculated stresses at fracture of the chips are found between 129 and 254 MPa. Calculation of stress estimates of the semicircular-shaped channels used in other studies [11-12] with fracture pressures of 120 to 360 bar, results in stresses of 94 to 252 MPa. Such stress levels are in the same range as seen in this study. For design 2, K_I is initially found between 0.31 and 0.58 MPa $m^{1/2}$, calculated by (2) and (3). To put this in perspective, average critical stress intensity factors of 0.75 MPa $m^{1/2}$ are seen for soda-lime glasses [23].

By comparing figure 2 and 8, one can see that there is a difference of design 1 and 2 when comparing fracture pressures, but not when comparing fracture stress. The lower fracture pressure of design 1 compared to design 2 can be explained by the geometric differences of the designs. By the use of the FEM models, no differences of the characteristic fracture stresses between the designs are seen. Given that the bond strength and flaw density distribution is the

same for both designs, the absence of any differences in the calculated stresses, figure 8, suggests that the flaw distribution is dense enough to produce a similar fracture pattern while having either a local, concentrated stressed point, or a global stress on the edge.

The long-term pressurization measurements give threshold pressures from which fracture does not occur within the scope of the test period. At temperatures between 11 and 38 °C, the highest pressure where the chips survived 1 week of constant pressurization, is about the same as the lowest measured fracture pressures seen during short-term measurements in this temperature region. This suggests that if the lower end of short-term fracture pressures is not exceeded, time reliability risks may be evaded in this temperature region. For the higher temperatures, of 80 to 125 °C, time dependent reliabilities can be a problem at pressures much lower than those seen at short-term measurements.

The estimates of the time of fracture by (5) show interesting results, figure 6. As the time estimation is sorely based on a circular crack front beginning at the cavity edge it does not take into account the presence of any flaws that can cause earlier fracture. Therefore, a chip that fractures much earlier than the estimate does most likely have a large defect. In the same sense, chips that fall close to the correlation line in figure 6 fit the estimation model well.

Comparisons of the calculated initial crack velocities between the average short-term fracture pressure and the long-term threshold pressures is in the order of 10^{-8} m/s and 10^{-10} m/s, respectively.

The determined short-term fracture pressure is not consistent with the assumed strength of glass. As determined by the speed measurements, figure 3, the crack front speed is in the order of 10^{-5} m/s. Such speeds are in the regime of slow crack growth. Together with the observation that moisture is found in the system also when the chips are pressurized using CO_2, and that the fracture stress intervals overlap while testing under either CO_2 or H_2O, slow crack growth affects even the short-term measurements. This is consistent with what has been seen while doing these types of measurements before by others [11]. To the authors knowledge, no investigation of the slow crack growth in high-density CO_2 have been made, but it is known that very low concentrations of H_2O in fluids can cause cracks to grow [24]. As crack velocity generally is dependent on the activity of water, this implies that rates are affected by both the effective partial pressure and the solubility of the H_2O in CO_2 system. The solubility of H_2O in CO_2 is a function of both temperature and pressure and is

strongly affected by other gas impurities [25]. While handling compressed gasses, the strong cooling from expansion can cause condensation of water in experimental setup if put in contact with air. The source of the water detected comes probably from residual moisture that has adhered to the inside of the tubing leading from the chip to the pump.

Figure 3 shows that a circular crack front is formed that dilate around the cavity as it progresses. As crack fronts are formed on both sides of the cavity, it suggests that multiple initiation points of crack propagation are present. This would then indicate a narrow flaw size distribution of high density. Crack initiation from bond interfaces is seen, but as the crack later propagates away from the interface, this suggests that the bonding is strong.

To design glass chips for high pressures with high reliability, several design considerations must be made. Stress concentrations must always be avoided, as it will be initiation points of the slow crack growth. Evading the sharp edge formed by single sided isotropic etching have been discussed in other studies and can be avoided by etching both wafers, thereby creating a circular wall [11]. This procedure does put high requirements on wafer alignment and as some misalignment always will be present, it does not evade the problem completely. If channel widths are kept small, higher pressures can be tolerated. By replacing (1) with an similar expression [15, 26] for straight channels, K_I can be estimated for such a case. A 200 μm wide channel pressurized to 500 bar with H_2O at room temperature should results in 0.32 MPa $m^{1/2}$. This would then correspond to a survivability of more than 1 week. To keep dimensions larger, approaches where the slow crack growth is inhibited should be explored. Studies have been conducted on how different advanced ceramics and glasses respond to delayed fracture [27] and as aluminosilicate and amorphous silica show crack growth at higher K_I [20], other materials choices less prone to crack growth could result in more durable chips. Further, long-term annealing of glass at temperatures around the wafer bonding temperatures used in this work, has been shown to cause phase separation of into silica rich and alkali-boron rich phases, making the glass more sensitive for crack growth [28]. It might therefore be reasonable to review bonding schemes. Other authors have tried to add hydrophobic silane coatings to stop H_2O from reaching the flaws on borosilicate glass rods [29]. However, they found no indication that such coatings hindered the environmental crack growth.

6. Conclusions

The long-term reliability of the bonded microfluidic chips is dependent on both the applied stress and the temperature. By using pressures slightly less than the lower ones observed by the short-term measurement schemes, a reliability of 1 week can be sustained for systems operating at 11 to 38 °C. When the temperature was increased to 80 °C, the pressure had to be reduced by 45% in order to still achieve a lifetime of 1 week. Estimations of the device lifetime were made, showing that the time of fractures agrees well with slow crack growth.

Acknowledgement

Funding from the Swedish Research Council (contract no. 2011-5037) is acknowledged as well as the funding for the laboratory facilities by Knut and Alice Wallenberg Foundation.

References

[1] Marre S, Roig, Y and Aymonier C 2012 Supercritical microfluidics: Opportunities in flow-through chemistry and materials science *J. Supercrit. Fluids* **66** 251–64

[2] Assmann N, Werhan H, Ładosz A and Rudolf von Rohr P 2013 Supercritical extraction of lignin oxidation products in a microfluidic device *Chem. Eng. Sci.* **99** 177-83

[3] Timko M T, Marre S and Maag A R 2016 Formation and characterization of emulsions consisting of dense carbon dioxide and water: Ultrasound *J. Supercrit. Fluids* **109** 51-60

[4] Marre S, Adamo A, Basak S, Aymonier C and Jensen K F 2010 Design and packaging of microreactors for high pressure and high temperature applications, *Ind. Eng. Chem. Res.* **49** 11310–20

[5] Luther S K, Schuster J J, Leipertz A and Braeuer A 2013 Microfluidic investigation into mass transfer in compressible multi-phase systems composed of oil, water and carbon dioxide at elevated pressure, *J. Supercrit. Fluids* **84** 121-31

[6] Thurmann S, Mauritz L, Heck C and Belder D 2014 High-performance liquid chromatography on glass chips using precisely defined porous polymer monoliths as particle retaining elements, *J. Chromatogr.* A **1370** 33-9

[7] Ciceri D and Nishi K and Stevens G W and Perera J M 2013 An Integrated UV-Vis Microfluidic Device for the Study of Concentrated Solvent Extraction Reactions, *Solvent Extr. Res. Dev., Jpn.* **20** 197 – 203

[8] Freiman S 2012 The fracture of glass: Past, present, and future *Int. J. Appl. Glass. Sci.* **3** 89–106

[9] Freiman S, Wiederhorn S M, and Mecholsky J J 2009 Environmentally enhanced fracture of glass: A historical perspective *J. Am. Ceram. Soc.* **92** 1371–82

[10] Ciccotti M 2009 Stress-corrosion mechanisms in silicate glasses *J. Phys. D: Appl. Phys.* **42**

[11] Tiggelaar R M, Benito-López F, Hermes D C, Rathgen H, Egberink R J M, Mugele F G, Reinhoudt D N, van den Berg A, Verboom W,and Gardeniers H J G E 2007 Fabrication, mechanical testing and application of high-pressure glass microreactor chips *Chem. Eng. J.* **131** 163–70

[12] Oosterbroek R E, Hermes D C, Kakuta M, Benito-Lopez F, Verboom W, Gardeniers J G E, van den Berg A, and Reinhoudt D N 2006 Fabrication and mechanical testing of glass chips for high pressure

synthetic or analytical chemistry. *Microsys. Technol.* **12** 450–4

[13] Huang Y, Vasan A S S, Doraiswami R, Osterman M, and Pecht M. 2012 MEMS reliability review. Device and Materials Reliability *IEEE Trans. Device Mater. Rel.* **12** 482–93

[14] Van Arsdell W W and Brown S B 1999 Subcritical crack growth in silicon MEMS. *J. Microelectromech. Syst* **8** 319–27

[15] Vallin Ö, Jonsson K and Lindberg U 2005 Adhesion quantification methods for wafer bonding. *Mater. Sci. Eng.*, R **50** 109-65

[16] Bennett S J, Devries K L, and Williams M L 1974 Adhesive fracture mechanics. *Int. J. Fract.* **10** 33–43

[17] Schott Technical Glass solutions, "BOROFLOAT® 33 – Mechanical Properties " datasheet, april 2016

[18] Köhler J, Jonsson K, Greek S and Stenmark L 2000 Weibull fracture probability for silicon wafer bond evaluation *J. Electrochem. Soc.* **147** 4683– 7

[19] Richard Å, Köhler J and Jonsson K 2002 Weibull fracture probability for characterisation of the anodic bond process. *Sens. Actuators*, A **99** 304–11

[20] Wiederhorn S M and Bolz L H 1970 Stress corrosion and static fatigue of glass *J. Am. Ceram. Soc.* **53** 543–8

[21] Wiederhorn S M, Fuller E R and Thomson R 1980 Micromechanisms of crack growth in ceramics and glasses in corrosive environments *Metal Science* **14** 450–8

[22] Pukh V P, Baikova L G, Kireenko M F and Tikhonova L V 2010 On the Kinetics of Crack Growth in Glass, On the kinetics of crack growth in glass, *Glass Phys. Chem*, **35** 560-6

[23] Geandier G, Denis S and Mocellin A 2003 Float glass fracture toughness determination by hertzian contact: experiments and analysis. *J. Non-Cryst. Solids* **318** 284–95

[24] Wiederhorn S M, Freiman S W, Fuller E R and Simmons C J 1982 Effects of water and other dielectrics on crack growth *J. Mater. Sci.* **17** 3460-78

[25] Ahmad M and Gersen S 2014 Water solubility in co2 mixtures: Experimental and modelling investigation. *Energy Procedia* **63** 2402–11

[26] Blom M T, Tas N R, Pandraud G, Chmela E, Gardeniers J G E, Tijssen R, Elwenspoek M and van den Berg A. 2001 Failure mechanisms of pressurized microchannels: model and experiments. *Microelectromech. Syst* **10** 158–64

[27] Choi S R, Nemeth N N and Gyekenyesi J P 2005 Exponential slow crack growth of glass and advanced ceramics—dynamic fatigue. *Fatigue. Fract. Eng. M.* **28** 489–97

[28] Simmons C J and Freiman S W 1980 Effects of phase separation on crack growth in borosilicate glass *J. Non-Cryst. Solids* **38–39** 503–508.

[29] Kirkpatrick R and Muhlstein C L 2007 Performance and durability of octadecyltrichlorosilane coated borosilicate glass *J. Non-Cryst. Solids* **353** 2624–37